BNL-107399-2015-JA

The effects of side-chain-induced disorder on the emission spectra and quantum yields of oligothiophene nano-aggregates: a combined experimental and MD-TDDFT study

Jiyun Hong[1], SuKyung Jeon[1], Janice J. Kim[1], Diane Devi[1], Kelly Chacon-Madrid[1], Wynee Lee1, Seung Moh Koo[1], J. Wildeman[2], M. Y. Sfeir[3] and L. A. Peteanu[1]

[1]Department of Chemistry, Carnegie Mellon University, 4400 Fifth Avenue Pittsburgh PA 15213

[2]Zernike Institute of Advanced Materials Nijenborgh 49747 AG Groningen, The Netherlands

[3]Center for Functional Nanomaterials (CFN), Brookhaven National Laboratories, Upton, NY 11973

Submitted to the Journal of Physical Chemistry A

November 2014

Center for Functional Nanomaterials

Brookhaven National Laboratory

U.S. Department of Energy
Office of Science, Basic Energy Sciences

Notice: This manuscript has been co-authored by employees of Brookhaven Science Associates, LLC under Contract No. DE-AC02-98CH10886 with the U.S. Department of Energy. The publisher by accepting the manuscript for publication acknowledges that the United States Government retains a non-exclusive, paid-up, irrevocable, world-wide license to publish or reproduce the published form of this manuscript, or allow others to do so, for United States Government purposes.

DISCLAIMER

This report was prepared as an account of work sponsored by an agency of the United States Government. Neither the United States Government nor any agency thereof, nor any of their employees, nor any of their contractors, subcontractors, or their employees, makes any warranty, express or implied, or assumes any legal liability or responsibility for the accuracy, completeness, or any third party's use or the results of such use of any information, apparatus, product, or process disclosed, or represents that its use would not infringe privately owned rights. Reference herein to any specific commercial product, process, or service by trade name, trademark, manufacturer, or otherwise, does not necessarily constitute or imply its endorsement, recommendation, or favoring by the United States Government or any agency thereof or its contractors or subcontractors. The views and opinions of authors expressed herein do not necessarily state or reflect those of the United States Government or any agency thereof.

This document is confidential and is proprietary to the American Chemical Society and its authors. Do not copy or disclose without written permission. If you have received this item in error, notify the sender and delete all copies.

The Effects of Side-Chain-Induced Disorder on the Emission Spectra and Quantum Yields of Oligothiophene Nano-Aggregates: A Combined Experimental and MD-TDDFT Study

Journal:	*The Journal of Physical Chemistry*
Manuscript ID:	jp-2014-04254a
Manuscript Type:	Special Issue Article
Date Submitted by the Author:	30-Apr-2014
Complete List of Authors:	Hong, Jiyun; Carnegie Mellon University, Chemistry Jeon, SuKyung; Carnegie Mellon University, Chemistry Kim, Janice; Carnegie Mellon University, Chemistry Devi, Diane; Carnegie Mellon University, Chemistry Chacon-Madrid, Kelly; Carnegie Mellon University, Chemistry Lee, Wynee; Carnegie Mellon University, Chemistry Koo, Seung; Carnegie Mellon University, Chemistry Wildeman, Jurjen; Zernike Institute of Advanced Materials, Polymer Chemistry and Bioengineering Sfeir, Matthew; Brookhaven National Laboratories, 3Center for Functional Nanomaterials Peteanu, Linda; Carnegie Mellon University , Chemistry Wen, Jin; Nanjing University, Chemistry and Chemical Engineering Ma, Jing; Nanjing University, Chemistry and Chemical Engineering

SCHOLARONE™
Manuscripts

The effects of side-chain-induced disorder on the emission spectra and quantum yields of oligothiophene nano-aggregates: a combined experimental and MD-TDDFT study

Jiyun Hong[1], SuKyung Jeon[1], Janice J. Kim[1], Diane Devi[1], Kelly Chacon-Madrid[1], Wynee Lee[1], Seung Moh Koo[1], J. Wildeman[2], M. Y. Sfeir[3] and L. A. Peteanu[1*]

[1]*Department of Chemistry, Carnegie Mellon University, 4400 Fifth Avenue Pittsburgh PA 15213*
[2]*Zernike Institute of Advanced Materials Nijenborgh 49747 AG Groningen, The Netherlands*
[3]*Center for Functional Nanomaterials (CFN), Brookhaven National Laboratories, Upton, NY 11973*

Jin Wen and Jing Ma[†]

Institute of Theoretical and Computational Chemistry, Key Laboratory of Mesoscopic Chemistry of MOE, School of Chemistry and Chemical Engineering, Nanjing University, Nanjing, 210093, P. R. China

Abstract

Oligomeric thiophenes are commonly-used components in organic electronics and solar cells. These molecules stack and/or aggregate readily under the processing conditions used to form thin films for these applications, significantly altering their optical and charge-transport properties. To determine how these effects depend on the substitution pattern of the thiophene main chains, nano-aggregates of three sexi-thiophene (6T) oligomers having different alkyl substitution patterns were formed using solvent poisoning techniques and studied using steady-state and time-resolved emission spectroscopy. The results indicate the substantial role played by the side-chain substituents in determining the emissive properties of these species. Both the measured spectral changes and their dependence on substitution are well modeled by combined quantum chemistry and molecular dynamics simulations. The simulations connect the side-chain-induced disorder, which determines the favorable chain packing configurations within the aggregates, with their measured electronic spectra.

*corresponding author: peteanu@cmu.edu

[†] majing@nju.edu.cn

Introduction

π-conjugated materials have garnered significant attention as the main component of organic electronics and solar cells. Important members of this class are alkyl-substituted poly-thiophenes and thiophene oligomers. In the production of organic electronic devices, these materials are cast from a highly-concentrated solution into a thin film. Because the chain conformation and the degree of aggregation of these materials in the precursor solution directly influence the film properties, studies of aggregation in solution are directly relevant to understanding thin-film characteristics.[1-4] The focus of the current study, oligomeric thiophenes, not only serve as models for the polymer form but are themselves used as the active component in organic field-effect transistors.[5-8] Numerous studies have focused on the photo-physics of this class of materials in solution-phase isolated chains,[9-12] nano-aggregates,[13-16] and thin films.[17-22]

This contribution explores how side-chain alkyl substituents affect aggregate optical and dynamical properties and how these properties can be successfully modeled using combined quantum chemistry and molecular dynamics (MD) simulations. In order to vary the substituent properties while maintaining the conjugated system at the same length, three sexi-thiophenes (6T) (Chart 1) are compared.

Several aspects of the electronic spectroscopy of thiophene nano-aggregates are typically explained by the exciton coupling model.[23, 24] Considering a minimal aggregate structure consisting of two coupled molecules, two classifications are possible based on whether the lower energy excitonic state results from the constructive (J-aggregate) or destructive (H-aggregate) combination of the two molecular transition moments. In the limit of strong coupling, the spectral consequences are red-shifted absorption and strong emission for J-aggregates and blue-shifted absorption with weak emission for H-aggregates. Extensions of this basic model,[25-28] have been used to interpret the spectroscopy of aggregates of oligomeric thiophenes[13, 18] and the polymer poly-3hexylthiophene (P_3HT).[29-31]

In this contribution, the effects of aggregation on the spectra and dynamics of three oligomeric thiophenes nano-aggregates (Chart 1) having distinct side-chain substitution patterns are explored. The solvent re-precipitation process used produces two types of aggregates: one similar to previously-reported oligothiophene H-aggregates[17, 19, 21, 22] and a second that is not readily classified within the basic exciton-coupling model. In addition, the impact of changing the alkyl-group substitution patterns on aggregate properties is explored both experimentally and through combined quantum chemistry and molecular dynamics simulations.

Methods

Solutions (1-5 μM) of all three oligomers in their monomeric forms were prepared in tetrahydrofuran (THF) by weighing out the amount needed to make the solution without serial dilution. Various aliquots of the THF solutions were added to 1 ml of de-ionized water to induce aggregation. Each solution was characterized *via* absorption and emission spectroscopies and by dynamic light scattering (DLS). For all three oligomers, the mean diameters (d) of the aggregates decreased with decreasing THF:water ratios (SI fig. 1). The highest values were in the range 600-1500 nm while the lowest ranged from 100-200 nm. Wavelength-resolved fluorescence lifetime decays (bandpass ±5 nm unless otherwise noted) were measured using a home-built spectrometer with excitation by a diode laser at 440 nm or 375 nm and detection using time correlated single photon counting (TCSPC, Picoquant 300) and a SPAD (MPD).[32] The effective time resolution is 200 ps. Higher time resolution (~ 100 fs) fluorescence decays were measured using fluorescence upconversion.[33]

The computational studies were performed utilizing two kinds of solvent models, implicit and explicit. The solvent effects on electronic structures were described by using the continuum dielectric model through quantum chemical calculations. Geometry optimization and frequency calculations were carried out to search for the optimized structures at the ground state S_0 at the density functional theory (DFT) level. To model the THF and water solvent molecules, the polarizable continuum model (PCM)[34] was

used with ε=7.43 and 78.36, respectively, in geometry optimizations. Time dependent density functional theory (TDDFT) was employed to calculate the absorption and emission spectra of monomers. Molecular structures of the first excited state were optimized at time-dependent DFT (TDDFT) level from starting geometries in the ground state. The excitation energies were calculated at TDDFT level in the ground-state geometries to simulate the absorption spectra. The emission spectra were simulated from the excitation energies at geometries in the first excited state by TDDFT calculations. In all DFT and TDDFT calculations the B3LYP functional[35-40] was used with the 6-31G* or 6-31+G* basis set as implemented in Gaussian 09 package.[41]

Molecular dynamics (MD) simulations with hundreds of discrete solvent molecules were employed to investigate the aggregate configurations in THF:water (0.1:1) solutions. The oligothiophene aggregates were simulated in a cubic box (with the periodic boundary condition), containing 20 oligothiophene chains, 50 tetrahydrofuran and 450 water molecules. MD simulations were performed in the canonical (NVT) ensemble with the polymer consistent force field (PCFF).[42] This force field has been successfully used to calculate the packing conformations of oligothiophenes in the amorphous phase,[43, 44] in various solutions,[45, 46] and on an Ag(111) surface.[47, 48] In order to reproduce the experimental conditions, we used a temperature of 298 K which was controlled by an Andersen[49] thermostat. The equations of motion were integrated by the velocity Verlet[50, 51] method with the time step of 1 fs. The 1 ns MD trajectories were collected after the equilibrium stage at 100 fs intervals. All dynamics simulations were performed in the Materials Studio program.[52]

Results and Discussion

Upon aggregation, the absorption maximum (λ_{abs}) of α-sexithiophene (α6T) shifts from 440 nm to higher energy (λ_{abs} =364 nm, +4745 cm^{-1} shift), as expected for strongly-coupled H-aggregates, and the spectral shape is radically altered (fig. 1). The asymmetrical band of the aggregate results from the overlap of at least three unique types of emitters as is demonstrated *via* the fluorescence excitation measurements described below. At relatively low percentages of water (*i.e.* 1:1 and 0.8:1 THF:water, fig. 2 and SI

fig. 2), the emission maxima (λ_{em}) of the aggregate (456 nm and 482 nm) and monomer (506 and 540 nm) overlap. As the water percentage increases, only the aggregate bands are visible (fig. 2). The two vibronic bands of the aggregate have similar spacing (1200 cm^{-1}) as in the monomer but are more nearly equal in intensity.

In addition to this relatively intense higher-energy band, extremely weak emission is observed in the 550-700 nm region (fig. 3). This red-shifted emission band appears in the same spectral region as that observed for α6T thin films[53] and corresponds well with that predicted for strongly-coupled H-aggregates.[28] However the blue-shifted aggregate emission has not been previously reported, to our knowledge. In principle, both the red- and blue-shifted emission could arise from a single aggregate type (same ground-state structure) or from different aggregate types presumably with different packing structures. The fluorescence excitation spectra described next support the latter interpretation.

Excitation spectra obtained by collecting at the emission maxima of the 'blue-emitting' (λ_{em} of 455 and 484 nm) and 'red-emitting' (λ_{em} = 592 nm) nano-aggregates of α6T are shown overlaid with the monomer and aggregate absorption spectra in fig. 4. The excitation spectrum of the 'red-emitting' aggregate overlays the sharp absorption transition at λ_{abs} ~ 360 nm. The excitation spectrum of the 'blue-emitting' aggregate is relatively broad (excitation spectrum maximum (λ_{exc}) ~ 380 nm) and overlays the asymmetrical tail of the aggregate absorption. Both excitation spectra also contain emission due to residual monomer that decreases as the percentage of water is increased. These spectra demonstrate that the asymmetrical absorption band shape of the α6T aggregates results from at least two spectrally-distinct aggregate bands with some contribution from residual monomer. These arise from two distinct ground-state aggregate structures.

The excited-state dynamics of the 'blue-emitting' species were probed at ps and fs resolution using an excitation wavelength of 370 nm. In aggregates that show unusual vibronic patterns (> 0.5:1 THF:water), the emission lifetimes collected at the 507, 540, and 587 nm vibronic bands are intermediate between those of the monomer and of the aggregate (Table 1 and fig. 5). At the highest percentage of water (< 0.5:1 THF:water),

the lifetime is ~350 ps and independent of collection wavelength (fig. 5). From these trends, we conclude that the anomalous vibronic structure of the aggregates seen at low percentages of water (*i.e.* 1:1 THF:water, fig. 2) is due to the co-existence of monomeric and aggregated chains in the solution. Notably, though the lifetime of the blue-emitting aggregate is only a factor of two shorter than the monomer, it is over an order of magnitude less emissive. One way to rationalize this discrepancy would be if there were additional sub-picosecond decay components not observable in the TCSPC data. However, no additional short-time decay components were observed at higher time resolution (fig. 6). We will return to this point later.

The additional alkyl side chains at the terminal positions in α, ω hexyl-6T (H6T, Chart 1) do not appreciably alter the spectrum or fluorescence lifetime (0.92-0.98 ns with 90-99% amplitude as measured by TCSPC, Table 2) of the monomer relative to α6T in the 500-600 nm region. However, an additional peak at 465 nm is observed (fig. 7) that could not be eliminated *via* dilution, sonication, drying the THF, or heating the sample. It is assigned to the aggregate because it increases in intensity, relative to the vibronic bands in the 500-600 nm region, with increased concentration (SI fig. 3). It also coincides with a band that appears when H6T is deliberately aggregated (see below) and it has a shorter lifetime (0.44 ns, 80% amplitude) than do the lower-energy vibronic bands (0.95 ns, 95% amplitude, fig. 8). Moreover, the fluorescence excitation spectrum of this band is somewhat blue-shifted from those collected at the lower-energy monomer emission bands (SI fig. 4).

As was seen for α6T, adding water to H6T in THF results in decreased emission in the monomer region (500-600 nm) and increased fluorescence at shorter wavelengths (fig. 7). At higher water percentages, the spectrum contains features indicative of both the monomer and the aggregate (see fig 7, 2:1 THF:water). Under these conditions, the emission lifetime increases with increasing collection wavelength (fig. 8), suggesting that the spectrum arises from a mixture of both monomeric and aggregated emitters. At the highest percentage of water examined (fig. 7, 0.5:1 THF:water), no emission is seen in the monomer spectral region and the lifetime is 250 ps independent of collection

wavelength (fig. 8 and Table 2). Similar dynamics are seen at higher time resolution (fig. 9).

The fluorescence spectrum of H6T nano-aggregates is very similar to that of the α6T aggregates (compare figs. 3 and 10). The most intense emission is in the region 450-500 nm or blue-shifted relative to the main monomer transitions (510 and 560 nm). Despite this similarity, the intensity of the 'blue-emitting' aggregate emission relative to the monomer is significantly higher in H6T than in α6T (compare figs. 2 and 7). In addition, there is very weak shoulder at lower energy (fig. 10, λ_{em} ~ 650 nm). The excitation spectrum obtained by collecting at 465 nm is blue shifted (λ_{exc} = 400 nm, fig. 11) relative to the monomer but less so than is the corresponding band in α6T (λ_{exc} =~380 nm, compare fig. 4 and 11). In addition, the excitation spectrum of H6T collected at 640 nm (fig. 11) contains a peak similar to that seen in the absorption/excitation spectra of α6T (compare fig. 11 to fig. 4). Consistent with this, excitation at 360 nm produces weak emission on the low-energy side of the main aggregate fluorescence spectrum ('red-emitting' aggregate) similar to that observed for α6T (compare figs. 3 and 10). Unfortunately, the 360 nm peak is poorly resolved in the absorption spectrum of aggregated H6T (fig. 11).

The behavior of didodecyl-sexithiophene (D6T) upon addition of poor solvent is qualitatively different from that described earlier for α6T and H6T. Though aggregation is clearly evident *via* DLS (SI fig. 1), the emission spectra are unchanged even at 90% water. This is similar to the findings of Ref. 15 in which a hexyl-substituted oligomer was studied. Moreover, the emission yields (fig. 12) and lifetimes of the D6T aggregates are similar to those of the monomer (0.97 ns versus 0.88 ns for the aggregates versus the monomer, data not shown) all at but the highest water percentages. At ~ 90% water, the quantum yield decreases by ~25% (fig. 12) and an additional shorter decay component (~200 ps, 20% amplitude, data not shown) is observed. This suggests that the drop in yield at the highest water percentages is due to the creation of an additional non-radiative channel.

Overall, the foregoing data demonstrate that the alkyl chain substitution pattern in 6T significantly affects its emission properties on aggregation. This is presumably due to differences in the favorable chain packing geometries between the three oligomers. The spectral and dynamical properties of α6T and H6T aggregates are the most similar with the important distinction that the emission of α6T is much more strongly quenched. The absence of spectral shifts in D6T upon aggregation suggests that side-chain substituents disfavor the formation of strongly-coupled aggregates, at least in solution-aggregated short oligomers.[15] Moreover, under our conditions, a blue-emitting aggregate is formed in α6T and H6T that, to our knowledge, has not been previously reported. In H6T, this aggregate gives rise to significant fluorescence intensity. Below, we elaborate upon each of these observations.

Regarding the spectral and structural properties of α6T and H6T nano-aggregates, the 'red-emitting' form most resembles the predominant species formed *via* vapor deposition or in thin films and that has been discussed in the literature.[17] Its spectral properties are consistent with those predicted for strongly-coupled H-aggregates.[24, 27, 28] The chains in thiophene H-aggregates are expected to be closely stacked (inter-chain spacing < 5 Å) and to adopt herringbone[54] or possibly co-facial packing. In contrast, the spectral and dynamical properties of the 'blue-emitting aggregates' are more consistent with weakly-coupled highly-disordered chains. Specifically, the fact that these aggregates absorb and emit at higher energy than the monomer suggests that their constituent chains are less planar and therefore have a shorter effective conjugation length (ECL) than the free monomer. Considering the known evolution in the positions of the absorption and emission spectra of oligothiophenes, the spectral features of the 'blue-emitting' aggregate are consistent with an ECL of ~ 4 thiophene rings.[43, 44] Moreover, the emission lifetime of thiophenes is known to be reduced from 0.9 to 0.35 when the conjugation length is decreased from 6 to 4 rings.[12] This mimics the reduction in lifetime between the monomer and the 'blue-emitting' aggregates that we report here (Tables 1 and 2).

Though the 'blue-emitting' aggregates formed by H6T and α6T are spectrally quite similar, they have significantly different emission efficiencies. The H6T aggregates are only a factor of ~4 less fluorescent than the monomer (fig. 7) while the α6T aggregates are over an order of magnitude less emissive than monomeric α6T (fig. 2). This striking difference in yields is seen despite the fact that the two 'blue-emitting' aggregates have very similar lifetimes. This is contrary to expectation if we assume that the radiative rates of the α6T and H6T aggregates are similar (as are those of the monomer). If so, the emission yield from both α6T and H6T blue-emitting aggregates should be comparable. The observed difference would then reflect a higher propensity of H6T to form the 'blue-emitting' rather than 'red-emitting' aggregates as compared to that of α6T. Consistent with this is the fact that the emission peaks associated with the 'red-emitting' aggregate (*i.e.* the H-aggregate band, fig. 10) are significantly less intense than the corresponding features in α6T (fig. 3). The results of TDDFT combined with MD simulations, described below, also predict that H6T aggregates formed in solution will be more structurally-disordered than α6T aggregates due to the influence of the alkyl side chains. Therefore, H6T is less likely than is α6T to achieve the ordered stacking characteristic of weakly-emissive H-aggregates.

The packing conformations of all three aggregates in THF:water solutions were studied *via* a series of MD simulations with a selected snapshot at 1ns presented for each in fig. 13. In the right-hand column, the THF and water solvent molecules are hidden to visualize the aggregates more clearly. The *α*6T aggregate structure contains more extended π-stacked regions than do the other two oligomer aggregates (fig. 13a). We note that the preferred stacking motif in nanoparticle aggregates appears to be co-facial rather than herringbone as was measured for crystalline α6T.[54] To determine the length of π-conjugation path in the *α*6T aggregates, the ECL was estimated from the number of thiophene rings in a successively coplanar π-conjugated backbone (SI fig. 5). The spectra were then calculated as the weighted average of TDDFT excitation energies in the ECL population from statistical analysis. TDDFT calculations on the most populated configuration averaged from MD trajectories predict a blue shift of ~70-90 nm in the *α*6T

aggregate absorption spectrum due to breaking of the π-conjugation length upon backbone bending and distortion in solution.

The theoretical description of the H6T system is more complicated than that of α6T because there are many possible conformations of H6T with *anti* or *syn* alignments of the neighboring thiophene rings (see SI figs 6 and 7). Among them, the most stable anti-H6T conformer (with all *anti* conformation) is ~4.4 kcal/mol lower in energy than that of the syn-H6T conformation (with an all-*syn* arrangement of thiophene rings). Based on the relative energy between these two conformations, the Boltzmann distribution yields an *anti/syn* ratio of ~19:1. Figure 13b shows a snapshot from an MD simulation of H6T (*anti:syn*=19:1) aggregates. The alkyl side chains in H6T make it difficult to judge the extent of packing of these aggregates directly from the 3D snapshot. Additional detailed information (torsion angle of 6T (α), interchain distance (d), inclination angle (θ) and orientation angle (β) between two different chains) relevant to the packing structures of these aggregates is therefore given (fig. 14). Though the structural parameters for H6T and α6T aggregates are similar, one important distinction is that the calculated packing density of the α6T aggregates is higher than that of either the H6T or D6T aggregates (fig. 13). The stronger chain-chain interactions in α6T that are implied by this result help explain both its propensity to form H-aggregates and its substantial loss of emission on aggregation (*vide supra*).

In comparison with α6T and H6T aggregates, the weakly-bound D6T chains pack in a very disordered fashion. A snapshot of the D6T aggregate simulation (fig. 13c) shows that the solvent molecules are evenly distributed within the periodic simulation box. In addition, numerous THF and water molecules are present *between* the D6T chains, implying that this oligomer does not form compact aggregates *via* solvent precipitation. This is consistent with the fact that aggregation is only observed when the percentage of water in the solution is very high (>80%).

Inter-chain separation distance is the parameter most frequently correlated with the degree of electronic coupling between chains and therefore to the magnitude of the spectral shifts on aggregation. It is interesting to note that the simulations predict similar

values of 5.0-5.5 Å for all three oligomer aggregates despite the fact that only α6T and H6T exhibit spectral shifts that are consistent with strong inter-chain coupling. This can be understood by examining the plots of the orientational angle distribution. Here, the peaks at 0 and 180 degrees indicate that the most prevalent structures are those in which all 6 rings overlap significantly. This is seen for α6T and, to a lesser degree for H6T. In the case of D6T, the majority of the chains stack in a cross-shaped pattern (see also fig. 13c). As a result, the overall electronic coupling between D6T chains in the aggregate is predicted to be weaker than in α6T and H6T, which is consistent with experiment.

Conclusions

Both the presence and substitution pattern of alkyl side chains significantly influence the electronic spectra and emission yields of sexi-thiophenes aggregated by solvent precipitation. These effects can be rationalized *via* TDDFT calculations on structures generated by MD simulations of the solvent-induced aggregation process. Two types of aggregates are identified, both with absorption bands that are at higher energies than the monomer. One gives rise to weak and highly Stokes shifted emission ('red-emitting aggregate') is assigned as a strongly-coupled H-aggregate based on a qualitative comparison with the model predictions of Spano and coworkers.[28] This is the predominant species in un-substituted α6T which forms tightly-packed and relatively well-ordered aggregate structures according to our MD simulations. A second species that shows relatively intense and weakly Stokes-shifted emission ('blue-emitting aggregate') is predominant in the H6T aggregate spectra. Our MD results indicate that the H6T aggregates are more disordered than α6T aggregates. This also suggests that the inter-chain interactions are weaker overall in the 'blue-emitting aggregate' than in the 'red-emitting aggregate' species. TDDFT calculations on the aggregate structures derived from MD suggest that the blue shifts in the aggregate excitation energies arise from the balance of two forces- a decrease in the ECL of the chains and an increase in the dispersion interaction. An aggregation-induced decrease in ECL is consistent with the blue shift of the absorption/emission spectra and the decreased emission lifetime the 'blue-emitting' α6T and H6T aggregates. Overall, these results demonstrate the

predictive power of a combined MD-TDDFT approach in modeling complex and disordered solution-phase aggregates of conjugated molecules.

Acknowledgements

L. A. P. acknowledges NSF CHE-1012529 for financial support. This work was performed in part at the Center for Functional Nanomaterials, Brookhaven National Laboratory, which is supported by the U.S. Department of Energy, Office of Basic Energy Sciences, under Contract No. DE-AC02-98CH10886. J. M. thanks the support from the National Natural Science Foundation of China (Grant Nos. 212901 , 21273102) and High Performance Computing Center of Nanjing University for providing the IBM Blade cluster system.

Supporting Information

The SI contains DLS data for all three aggregate types, additional emission spectra of the α6T aggregates, and the concentration dependence of the H6T emission and excitation spectra. From MD results, the ECL for the three aggregate types is also given. In addition, the structural properties of aggregates formed from the *syn* and *anti* forms of 6HT are compared. This material is available free of charge *via* the Internet at http://pubs.acs.org.

References

1. Nguyen, T.-Q.; Doan, V. Schwartz, B. J., Conjugated Polymer Aggregates in Solution: Control of Interchain Interactions. *J. Chem. Phys.* **1999**, *110*, 4068.
2. Nguyen, T.-Q.; Kwong, R. C.; Thompson, M. E. Schwartz, B. J., Improving the Performance of Conjugated Polymer-based Devices by Control of Interchain Interactions and Polymer Film Morphology. *App. Phys. Lett.* **2000**, *76*, 2454.
3. Schwartz, B. J., Conjugated Polymers as Molecular Materials: How Chain Conformation and Film Morphology Influence Energy Transfer and Interchain Interactions. *Ann. Rev. Phys. Chem.* **2003**, *54*, 141.
4. Brazard, J.; Ono, R. J.; Bielawski, C. W.; Barbara, P. F. Vanden Bout, D. A., Mimicking Conjugated Polymer Thin-Film Photophysics with a Well-Defined Triblock Copolymer in Solution. *J. Phys. Chem. B* **2013**, *117*, 4170.
5. Fichou, D.; Horowitz, G. Garnier, F., Extended Oligothiophenes: New Materials for Molecular Electronics. *Mol. Cryst. Liq. Cryst. Sci. Tech. Section A* **1992**, *217*, 193.
6. Fichou, D., Structural Order in Conjugated Oligothiophenes and its Implications on Opto-Electronic Devices. *J. Mat. Chem.* **2000**, *10*, 571.
7. Murphy, A. R. Fréchet, J. M. J., Organic Semiconducting Oligomers for Use in Thin Film Transistors. *Chem. Rev.* **2007**, *107*, 1066.
8. Mishra, A. Bäuerle, P., Small Molecule Organic Semiconductors on the Move: Promises for Future Solar Energy Technology. *Angew. Chem.* **2012**, *51*, 2020.
9. Chosrovian, H.; Rentsch, S.; Grebner, D.; Dahm, D. U.; Birckner, E. Naarmann, H., Time-resolved Fluorescence Studies on Thiophene Oligomers in Solution. *Synth. Met.* **1993**, *60*, 23.
10. Grebner, D.; Helbig, M. Rentsch, S., Size-Dependent Properties of Oligothiophenes by Picosecond Time-Resolved Spectroscopy. *J. Phys Chem.* **1995**, *99*, 16991.
11. Becker, R. S.; Seixas de Melo, J.; Maçanita, L. Elisei, F., Comprehensive Investigation of the Solution Photophysics and Theoretical Aspects of Oligothiophenes with One to Seven Rings. *Pure and Appl. Chem* **1995**, *67*, 9.

12. Becker, R. S.; Seixas de Melo, J.; Maçanita, L. Elisei, F., Comprehensive Evaluation of the Absorption, Photophysical, Energy Transfer, Structural, and Theoretical Properties of α–Oligothiophenes with One to Seven Rings. *J. Phys. Chem.* **1996**, *100*, 18683.

13. Westenhoff, S.; Abrusci, A.; Feast, W. J.; Henze, O.; Kilbinger, F. M.; Schenning, A. P. H. J. Silva, C., Supramolecular Electronic Coupling in Chiral Oligothiophene Nanostructures. **2006**, *18*, 1281.

14. Ellinger, S.; Kreyes, A.; Ziener, U.; Hoffmann-Richter, C.; Landfester, K. Möller, M., Aggregation Phenomena of Long α– and α, ω–Substituted Oligothiophenes-the Effect of Branched vs. Linear End-Groups. *Eur. J. Org. Chem.* **2007**, *2007*, 5686.

15. Nepomnayashchii, A. B.; Ono, R. J.; Lyons, D. M.; Sessler, J. L.; Bielawski, C. W. Bard, A. J., Oligothiophene Nanoparticles: Photophysical and Electrogenerated Luminescence Studies. *J. Phys Chem. Lett.* **2012**, *3*, 2035.

16. Ostrowski, D. P.; Lytwak, L. A.; Mejia, M. L.; Stevenson, K. J.; Holliday, B. J. Vanden Bout, D. A., The Effects of Aggregation on Electronic and Optical Properties of Oligothiophene Particles. *ACS Nano* **2012**, *6*, 5507.

17. Yassar, A.; Valat, P.; Wintgens, V.; Hmyene, M.; Deloffre, F.; Horowitz, G.; Srivastava, P. Garnier, F., Structural Control of the Optical Properties of Thin Films of Oligothiophenes. *Synth. Met.* **1994**, *67*, 277.

18. Hamano, K.; Kurata, T.; Kubota, S. Koezuka, H., Organic Molecular Beam Deposition of α-Sexithienyl. *Jpn. J. Appl. Phys.* **1994**, *33*, 1031.

19. Oelkrug, D.; Egelhaaf, H.-J.; Worrall, D. R. Wilkinson, F., Fluorescence Yields and Molecular Orientation of Thin Organic Films: Vapor-Deposited Oligothiophenes α3T-α8T. *J. Fluor.* **1995**, *5*, 165.

20. Oelkrug, D.; Egelhaaf, H.-J.; Gierschner, J. Tompert, A., Electronic Deactivation in Single Chains, Nano-aggregates, and Ultrathin Films of Conjugated Oligomers. *Synth. Met.* **1996**, *76*, 249.

21. Taliani, C. Blinov, L. M., The Electronic Structure of Solid α-Sexithiophene. *Adv. Mat.* **1996**, *8*, 353.

22. Mei, P.; Murgia, M.; Taliani, C.; Lunedei, E. Muccini, M., Luminescence Quantum Yield of Molecular Aggregates and Excitons in α–Sexithienyl Thin Films at Variable Temperature. *J. App. Phys.* **2000**, *88*, 5158.

23. Davydov, A. S., Theory of Molecular Excitons**1962**, New York: McGraw-Hill.

24. McRae, E. G. Kasha, M., The Molecular Exciton Model, in Physical Processes in Radiation Biology**1964**, Academic Press: New York. 23.

25. Siddiqui, S. Spano, F. C., H- and J-Aggregates of Conjugated Polymers and Oligomers. A Theoretical Investigation. *Chem. Phys. Lett.* **1999**, *308*, 99.

26. Beljonne, D.; Cornil, J.; Silbey, R.; Millié, P. Bredas, J. L., Interchain Interactions in Conjugated Materials: The Exciton Model versus the Supermolecular Approach *J. Chem. Phys.* **2000**, *112*, 4749.

27. Spano, F. C., Excitons in Conjugated Oligomer Aggregates, Films, and Crystals. *Ann. Rev. Phys. Chem.* **2006**, *57*, 217.

28. Spano, F. C., The Spectral Signatures of Frenkel Polarons in H- and J-Aggregates. *Acc. Chem . Res.* **2010**, *43*, 429.

29. Clark, J.; Silva, C.; Friend, R. H. Spano, F. C., Role of Intermolecular Coupling in the Photophysics of Disordered Organic Semiconductors: Aggregate Emission in Regioregular Polythiophene. *Phys. Rev. Lett.* **2007**, *98*, 206406/1.

30. Niles, E. T.; D., R. J.; Yamagata, J.; Wise, A. J.; Spano, F. C.; Moule, A. J. K., G. J., J-Aggregate Behavior in Poly-3-hexylthiophene Nanofibers. *J. Phys. Chem. Lett.* **2012**, *3*, 259.

31. Baghgar, M.; Pentzer, E.; Wise, A. J.; Labastide, J. A.; Emrick, T. Barnes, M. D., Cross-Linked Functionalized Poly(3-hexylthiophene) Nanofibers with Tunable Excitonic Coupling. *ACS Nano* **2013**, *7*, 8917.

32. Sherwood, G. A.; Cheng, R.; Smith, T. M.; Werner, J. H.; Shreve, A. P.; Peteanu, L. A. Wildeman, J., Aggregation Effects on the Emission Spectra and Dynamics of Model Oligomers of MEH-PPV. *J. Phys. Chem. C* **2009**, *113*, 18851.

33. Huang, J.-S.; Goh, T.; Li, X.; Sfeir, M. Y.; Bielinski, E. A.; Tomasulo, S.; Lee, M. L.; Hazari, N. Taylor, A. D., Polymer Bulk Heterojunction Solar Cells Employing Förster Resonance Energy Transfer *Nature Photonics* **2013**, *7*, 479.

34. Foresman, J. B.; Keith, T. A.; Wiberg, K. B.; Snoonian, J. Frisch, M. J., Solvent Effects. 5. Influence of Cavity Shape, Truncation of Electrostatics, and Electron Correlation on ab Initio Reaction Field Calculations. *J. Phys Chem* **1996**, *100*, 16098.

35. Dirac, P. A. M., Quantum Mechanics of Many-Electron Systems. *Proc. Royal Soc. (London) A* **1929**, *123*, 714.

36. Slater, J. C., A Simplification of the Hartree-Fock Method. *Phys. Rev.* **1951**, *81*, 385.

37. Vosko, S. H.; Wilk, L. Nusair, M., Accurate Spin-Dependent Electron Liquid Correlation Energies for Local Spin Density Calculations: a Critical Analysis. *Can. J. Phys.* **1980**, *58*, 1200.

38. Becke, A. D., Density-Functional Exchange-Energy Approximation with Correct Asymptotic Behavior. *Phys. Rev. A* **1988**, *38*, 3098.

39. Lee, C.; Yang, W. Parr, R. G., Development of the Colle-Salvetti Correlation-Energy Formula into a Functional of the Electron Density. *Phys. Rev. B* **1988**, *37*, 785.

40. Becke, A. D., Density-Functional Thermochemistry. III. The Role of Exact Exchange. *J. Chem. Phys.* **1993**, *98*, 5648.

41. Frisch, M. J.; Trucks, G. W.; Schlegel, H. B.; Scuseria, G. E.; Robb, M. A.; Cheeseman, J. R.; Scalmani, G.; Barone, V.; Mennucci, B.; Petersson, G. A.; Nakatsuji, H.; Caricato, M.; Li, X.; Hratchian, H. P.; Izmaylov, A. F.; Bloino, J.; Zheng, G.; Sonnenberg, J. L.; Hada, M.; Ehara, M.; Toyota, K.; Fukuda, R.; Hasegawa, J.; Ishida, M.; Nakajima, T.; Honda, Y.; Kitao, O.; Nakai, H.; Vreven, T.; Montgomery, J., J. A.; Peralta, J. E.; Ogliaro, F.; Bearpark, M.; Heyd, J. J.; Brothers, E.; Kudin, K. N.; Staroverov, V. N.; Kobayashi, R.; Normand, J.; Raghavachari, K.; Rendell, A.; Burant, J. C.; Iyengar, S. S.; Tomasi, J.; Cossi, M.; Rega, N.; Millam, J. M.; Klene, M.; Knox, J. E.; Cross, J. B.; Bakken, V.; Adamo, C.; Jaramillo, J.; Gomperts, R.; Stratmann, R. E.; Yazyev, O.; Austin, A. J.; Cammi, R.; Pomelli, C.; Ochterski, J. W.; Martin, R. L.; Morokuma, K.; Zakrzewski, V. G.; Voth, G. A.; Salvador, P.; Dannenberg, J. J.; Dapprich, S.;

Daniels, A. D.; Farkas, J. B.; Foresman, J. B.; Ortiz, J. V.; Cioslowski, J. Fox, D. J., Gaussian 09, Revision B.01, **2009**, Gaussian, Inc.: Wallingford CT.

42. Sun, H., Ab Initio Calculations and Force Field Development for Computer Simulation of Polysilanes. *Macromol.* **1995**, *28*, 701.
43. Zhang, G.; Pei, Y.; Ma, J.; Yin, K. C.-L., C., Packing Structures and Packing Effects on Excitation Energies of Amorphous Phase Oligothiophenes. *J. Phys. Chem. B* **2004**, *108*, 6988.
44. Zhang, G.; Ma, J. Wen, J., Interchain Impacts on Electronic Structures of Heterocyclic Oligomers and Polymers Containing Group 14, 15, and 16 Heteroatoms:□ Quantum Chemical Calculations in Combination with Molecular Dynamics Simulations. *J. Phys. Chem. B* **2007**, *111*, 11670.
45. Meng, S.; Ma, J. Y., J., Solvent Effects on Electronic Structures and Chain Conformations of α-Oligothiophenes in Polar and Apolar Solutions. *J. Phys. Chem. B* **2007**, *112*, 4128.
46. Meng, S. Ma, J., Solvatochromic Shift of Donor-Acceptor Substituted Bithiophene in Solvents of Different Polarity:□ Quantum Chemical and Molecular Dynamics Simulations. *J. Phys. Chem. B* **2007**, *112*, 4313.
47. Wen, J. Ma, J., The Role of Substrate in Packing Structures of Sexithiophenes on Ag (111) Surface: Molecular Dynamics Simulations and Quantum Chemical Calculations. *J. Theor. Comput. Chem.* **2009**, *8*, 677.
48. Wen, J. Ma, J., Oligothiophene Template Effects on Packings and Orientations of C60 Molecules on Ag(111) Surface. *Langmuir* **2010**, *26*, 5595.
49. Andersen, H. C., *J. Chem. Phys.* **1980**, *72*, 2384.
50. Verlet, L., Computer "Experiments" on Classical Fluids. I. Thermodynamical Properties of Lennard-Jones Molecules. *Phys. Rev.* **1967**, *159*, 98.
51. Verlet, L., "Experiments" on Classical Fluids. II. Equilibrium Correlation Functions. *Phys. Rev.* **1967**, *165*, 201.
52. Studio, M., **2006**, Accelrys Inc.: San Diego.
53. Yassar, A.; Horowitz, G.; Valat, P.; Wintgens, V.; Hmyene, M.; Deloffre, F.; Srivastava, P.; Lang, P. Garnier, F., Exciton Coupling Effects in the Absorption

and Photoluminescence of Sexithiophene Derivatives. *J. Phys. Chem.* **1995**, *99*, 9155.

54. Horowitz, G.; Bachet, B.; Yassar, A.; Lang, P.; Demanze, F.; Fave, J.-L. Garnier, F., Growth and Characterization of Sexithiophene Single Crystals. *Chem. Mat.* **1995**, *7*, 1337.

Charts

Chart 1 Sexithiophene structures used in this work. For α6T, R_1 and R_2 are H. For H6T, R_1 is C_6H_{13} and R_2 is H. For D6T, R_1 is H and R_2 is $C_{12}H_{25}$.

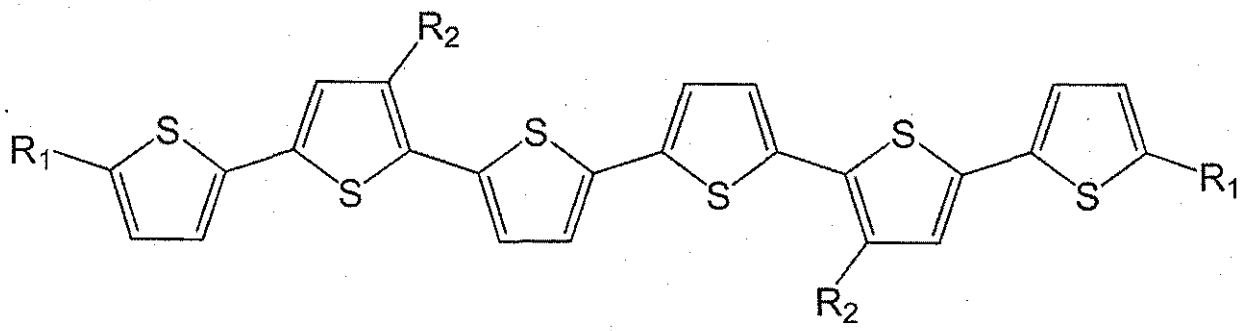

Chart 1 Sexithiophene structures used in this work. For α6T, R_1 and R_2 are H. For H6T, R_1 is C_6H_{13} and R_2 is H. For D6T, R_1 is H and R_2 is $C_{12}H_{25}$.

Figures

Fig. 1 Absorption spectra of monomeric and aggregated α6T.

Fig. 2 Emission of monomeric and aggregated α6T. The intensities have been scaled by the monomer dilution factor in the THF:water mixtures. The monomer spectrum is divided by 40 to facilitate comparison.

Fig. 3 Emission spectrum of a suspension of α6T aggregates exciting at 370 nm. The features corresponding to the 'blue-emitting' aggregates lie in the 450-500 nm region. The vibronic bands of the 'red-emitting' aggregate spectrum are identified by the arrows.

Fig 4 Excitation spectra (solid lines) of α6T aggregates formed in THF:water ratios of 1:1 (left), 0.8 :1 (middle), and 0.5:1 THF:water (right) color coded by collection wavelength. Absorption spectra of α6T monomer (dotted line) and aggregates (dash dot line) are also shown.

Fig 5. Fluorescence decays (symbols) and fits (solid lines) for various α6T aggregate preparations collected at the vibronic peaks of the emission spectra (± 5 nm bandpass). Emission decays collected at 460 nm and 480 nm (not shown) were identical within experimental error. Data was obtained with 375 nm excitation using TCSPC.

Fig 6 Normalized fluorescence decays and fits for aggregated α6T obtained using fluorescence upconversion with 370 nm excitation. Collection wavelengths are shown (± 5 nm).

Fig. 7 Emission of monomeric and aggregated H6T. All aggregate intensities have been scaled by the monomer dilution factor in the corresponding THF:water mixtures.

Fig. 8 Fluorescence decays (symbols) and fits (solid lines) for the H6T monomer (left) and various H6T aggregate preparations collected at the vibronic peaks of the emission spectra (± 5 nm bandpass). Data was obtained with 375 nm excitation using TCSPC.

Fig. 9 Normalized fluorescence decays and fits for aggregated H6T obtained using fluorescence upconversion with 370 nm excitation. Collection wavelengths are shown (± 5 nm).

Fig 10. Emission spectrum of a suspension of H6T aggregates exciting at 370 nm. The features corresponding to the 'blue-emitting' aggregates lie in the 450-500 nm region. The emission region of the 'red-emitting' aggregate is identified by the arrow.

Fig 11. Excitation spectra (solid lines) of H6T aggregates formed in 0.1:1 THF:water color coded by collection wavelength. Absorption spectra of H6T monomer (dashed line) and aggregates (dot line) are also shown.

Fig 12. Emission of monomeric and aggregated D6T. All aggregate intensities have been scaled by the monomer dilution factor in the corresponding THF:water mixtures.

Fig. 13 MD snapshots of nano-aggregates. Solvent molecules are hidden in the right-hand column to show the packing structures.

Fig. 14 Statistical analysis of the nano-aggregate packing structures from MD trajectories.

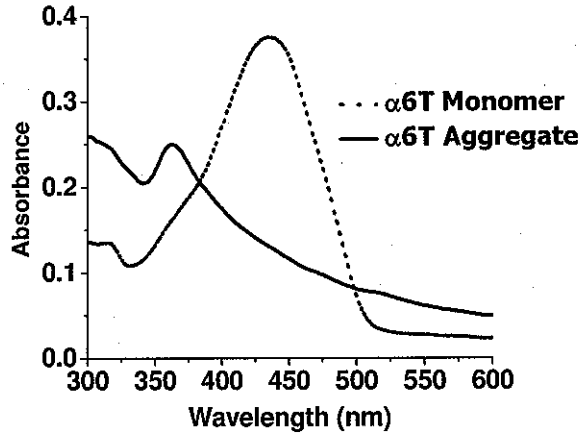

Fig. 1 Absorption spectra of monomeric and aggregated α6T.

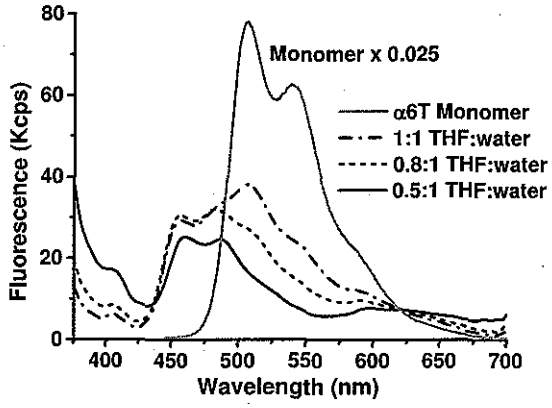

Fig. 2 Emission of monomeric and aggregated α6T. The intensities have been scaled by the monomer dilution factor in the THF:water mixtures. The monomer spectrum is divided by 40 to facilitate comparison.

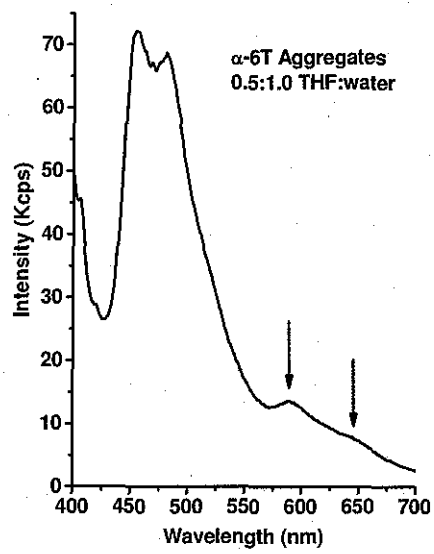

Fig. 3 Emission spectrum of a suspension of α6T aggregates exciting at 370 nm. The features corresponding to the 'blue-emitting' aggregates lie in the 450-500 nm region. The vibronic bands of the 'red-emitting' aggregate spectrum are identified by the arrows.

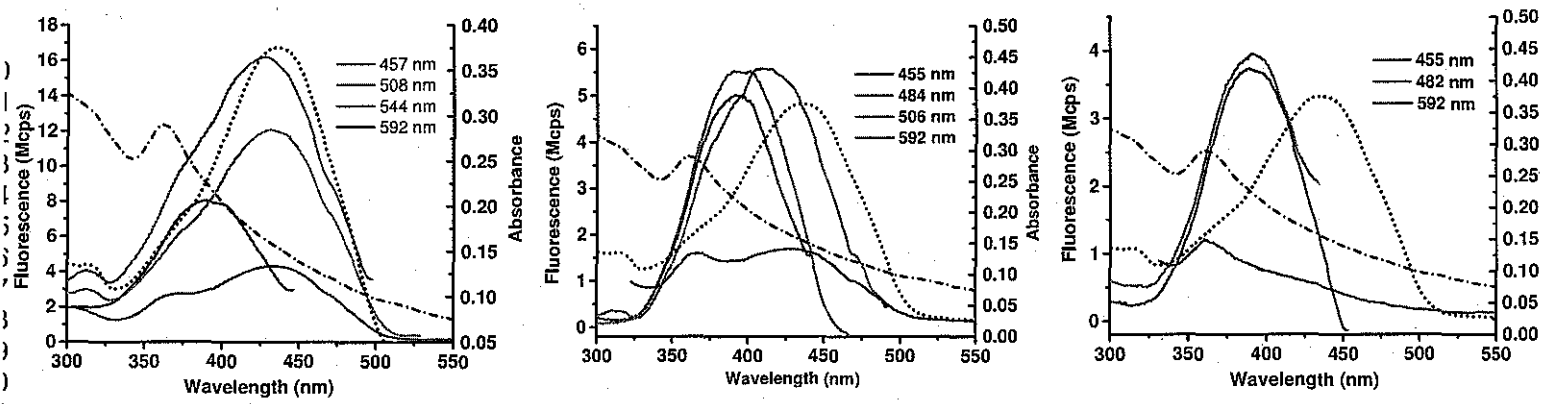

Fig 4 Excitation spectra (solid lines) of α6T aggregates formed in THF:water ratios of 1:1 (left), 0.8 :1 (middle), and 0.5:1 THF:water (right) color coded by collection wavelength. Absorption spectra of α6T monomer (dotted line) and aggregates (dash dot line) are also shown.

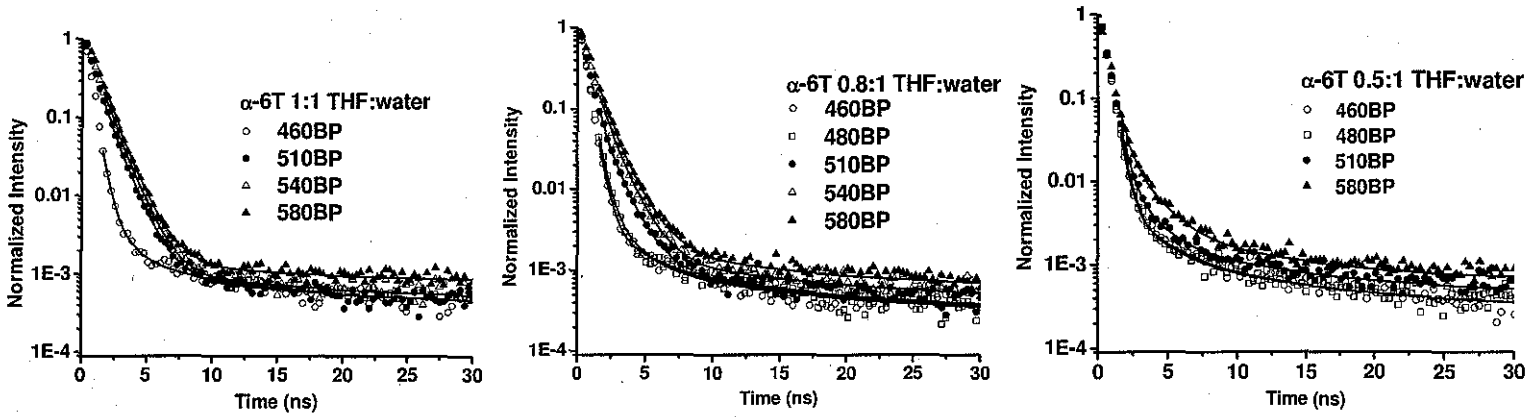

Fig 5. Fluorescence decays (symbols) and fits (solid lines) for various α6T aggregate preparations collected at the vibronic peaks of the emission spectra (± 5 nm bandpass). Emission decays collected at 460 nm and 480 nm (not shown) were identical within experimental error. Data was obtained with 375 nm excitation using TCSPC.

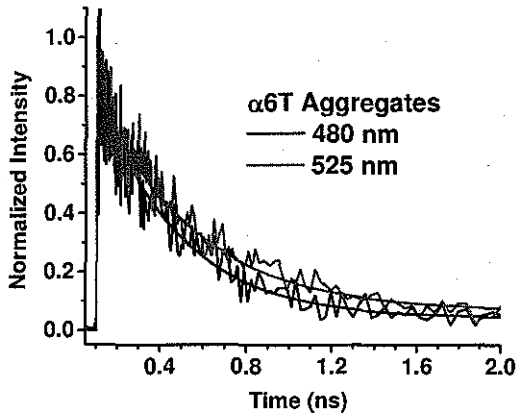

Fig 6 Normalized fluorescence decays and fits for aggregated α6T obtained using fluorescence upconversion with 370 nm excitation. Collection wavelengths are shown (± 5 nm).

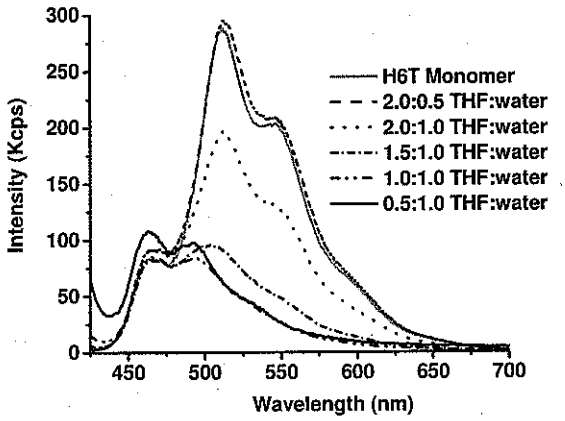

Fig. 7 Emission of monomeric and aggregated H6T. All aggregate intensities have been scaled by the monomer dilution factor in the corresponding THF:water mixtures.

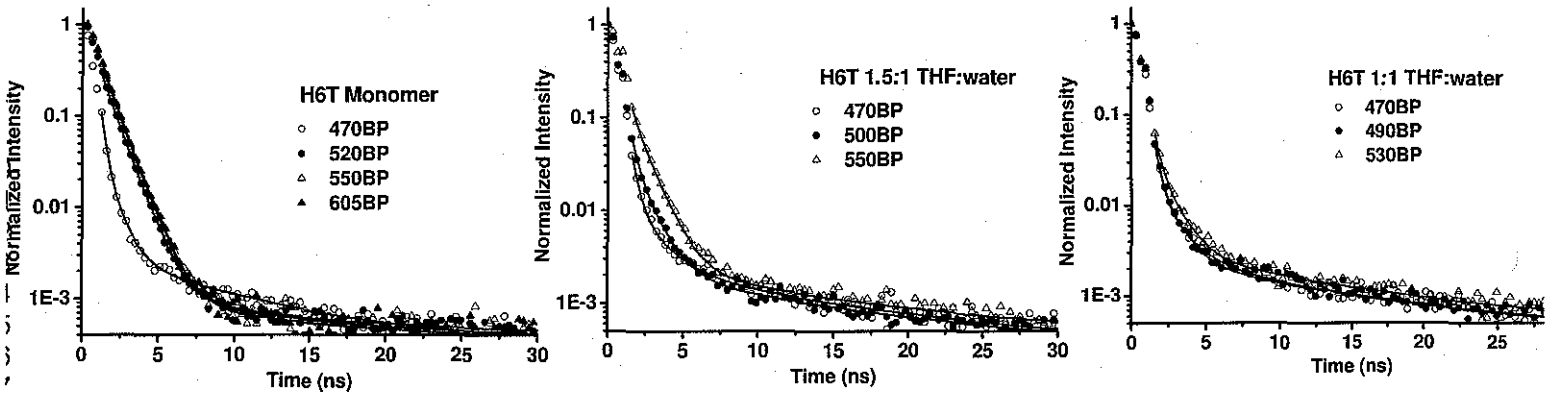

Fig. 8 Fluorescence decays (symbols) and fits (solid lines) for the H6T monomer (left) and various H6T aggregate preparations collected at the vibronic peaks of the emission spectra (± 5 nm bandpass). Data was obtained with 375 nm excitation using TCSPC.

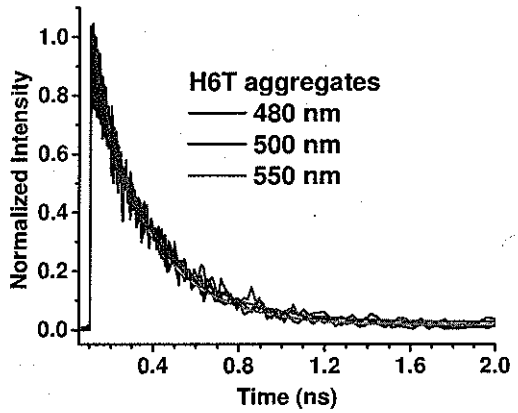

Fig. 9 Normalized fluorescence decays and fits for aggregated H6T obtained using fluorescence upconversion with 370 nm excitation. Collection wavelengths are shown (± 5 nm).

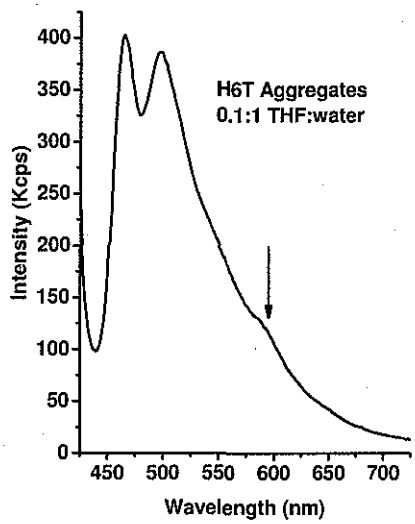

Fig 10. Emission spectrum of a suspension of H6T aggregates exciting at 370 nm. The features corresponding to the 'blue-emitting' aggregates lie in the 450-500 nm region. The emission region of the 'red-emitting' aggregate is identified by the arrow.

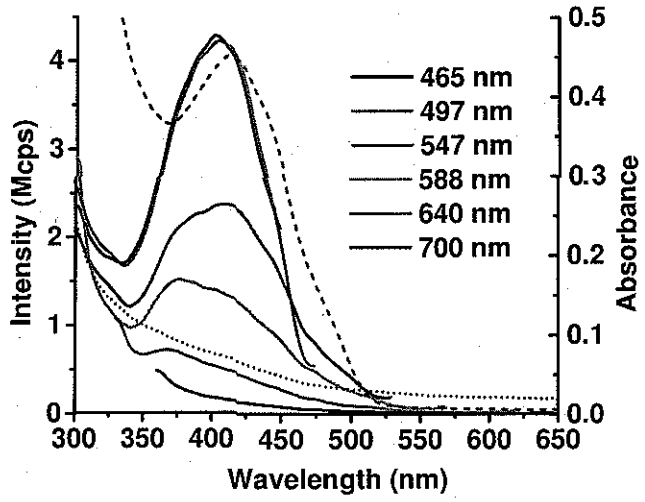

Fig 11. Excitation spectra (solid lines) of H6T aggregates formed in 0.1:1 THF:water color coded by collection wavelength. Absorption spectra of H6T monomer (dashed line) and aggregates (dot line) are also shown.

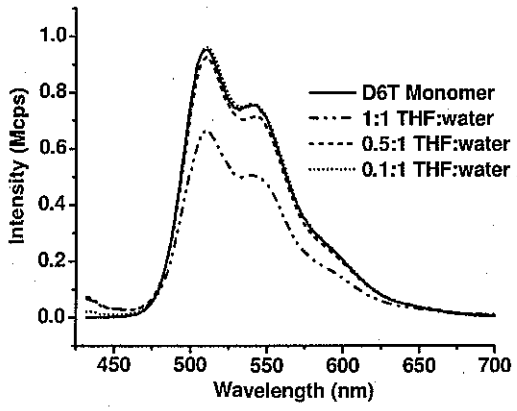

Fig 12. Emission of monomeric and aggregated D6T. All aggregate intensities have been scaled by the monomer dilution factor in the corresponding THF:water mixtures.

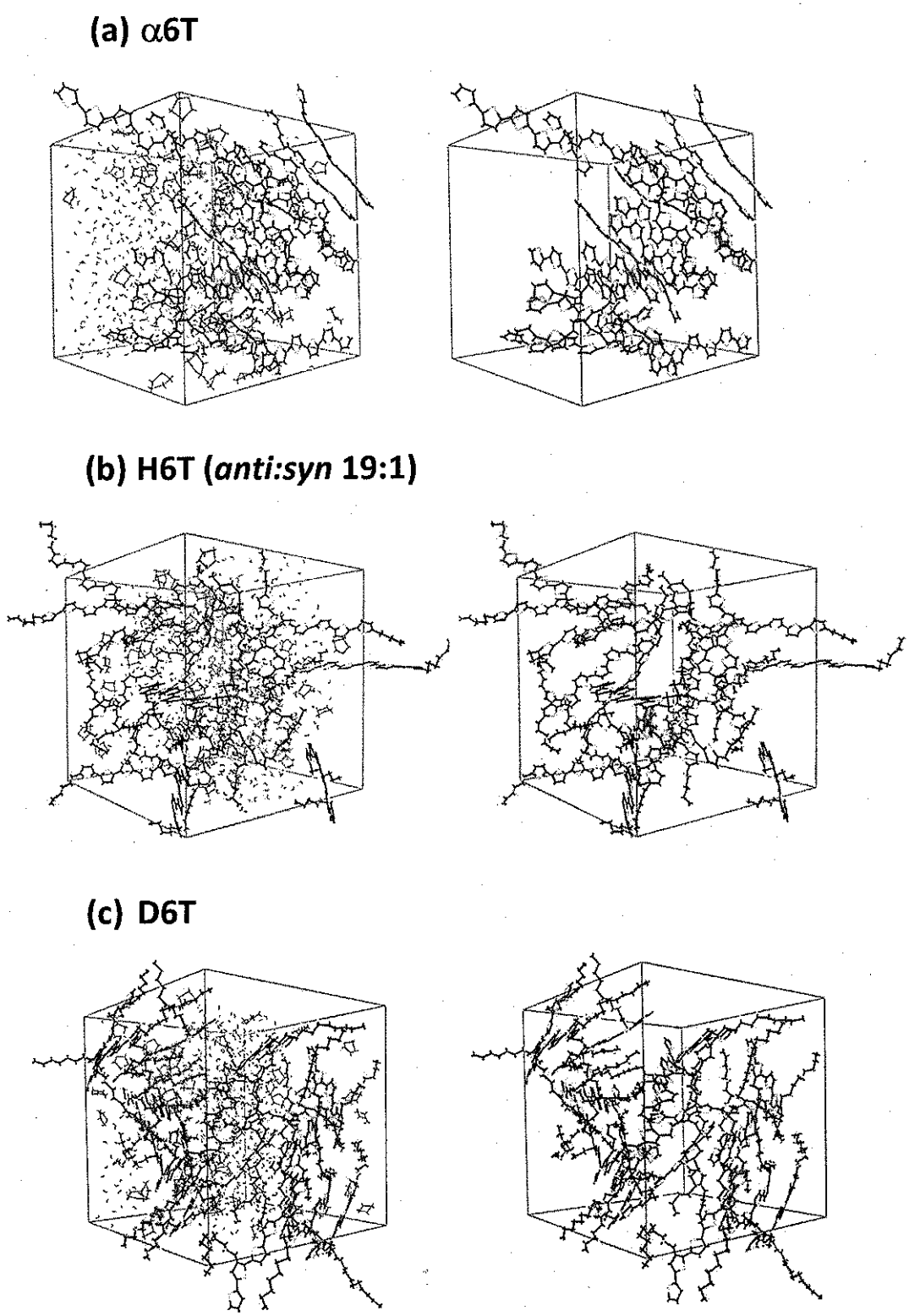

Fig. 13 MD snapshots of nano-aggregates. Solvent molecules are hidden in the right-hand column to show the packing structures.

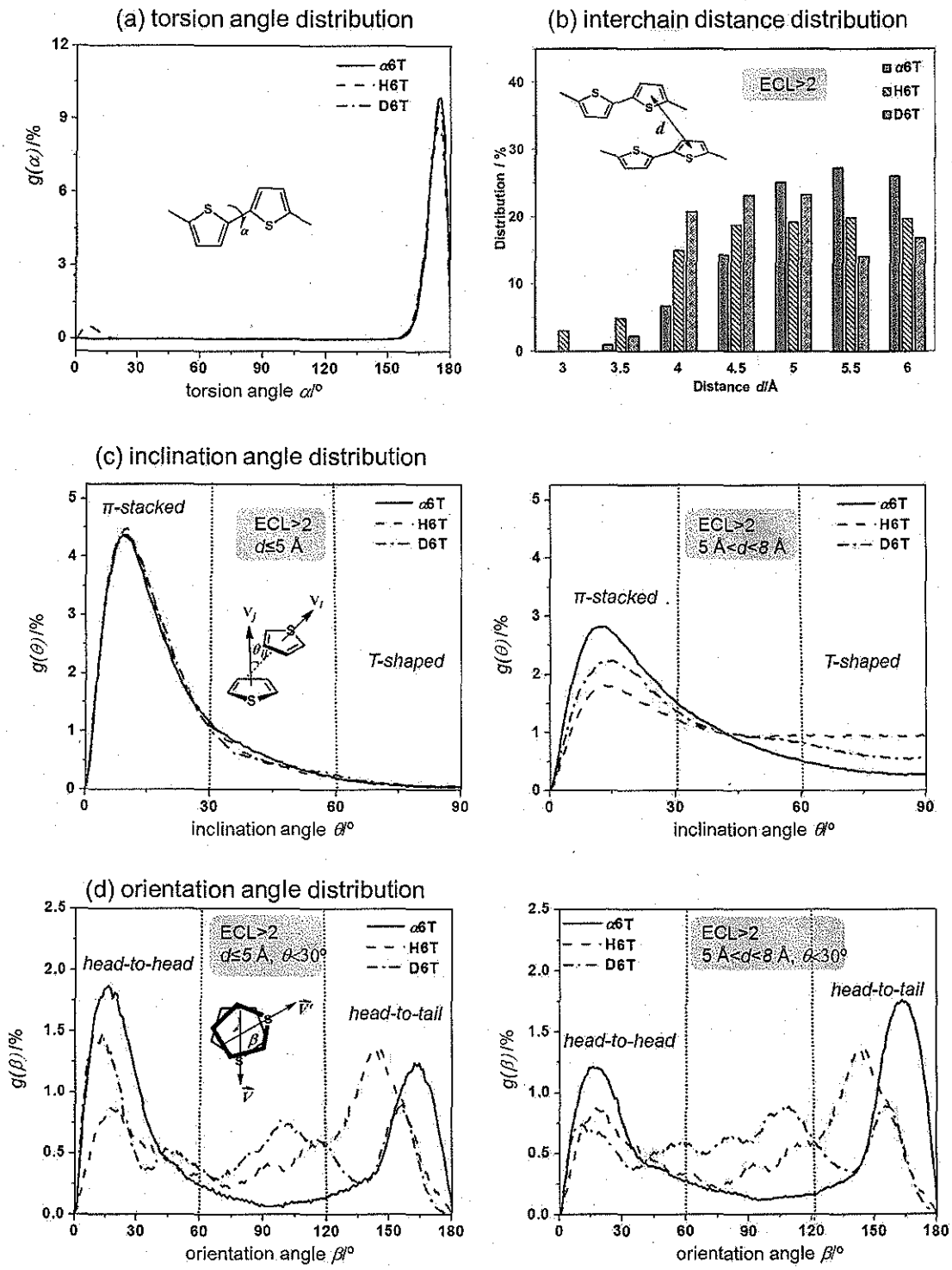

Fig. 14 Statistical analysis of the nano-aggregate packing structures from MD trajectories.

Tables

Table 1 Fluorescence lifetimes of α6T monomer and THF:water aggregates as a function of emission wavelength.

Table 2 Fluorescence lifetimes of H6T monomer and THF:water aggregates as a function of emission wavelength.

Table 1: Fluorescence lifetimes of α6T monomer and THF:water aggregates as a function of emission wavelength.

THF:water	460 nm[a]	510 nm	540 nm	580 nm
Monomer	-	0.94 (99.9)[b]	0.94 (99.9)	0.94 (99.9)
	0.41 (88)	0.73 (52.5)	0.79 (50.9)	0.93 (89)
1:1	1.3 (10)	1.17 (47)	1.17 (48.8)	1.54 (11.8)
	8.2 (2)	10.4 (0.5)	10.4 (0.3)	11.6 (0.2)
	0.46 (95)	0.54 (55)	0.66 (54)	0.76 (64)
0.8:1	2.7 (4)	1.2 (44)	1.2 (45)	1.3 (35)
	12 (1)	9.3 (1)	9.7 (1)	9.0 (1)
	0.44 (93)	0.54 (55)		0.76 (64)
0.5:1	2.4 (5)	1.18 (44)	-	1.3 (35)
	10.5 (2)	9.3 (1)		9.0 (1)

[a] All wavelengths are ± 5 nm. Monomer lifetimes are fit to a double exponential function while aggregate decays are fit to a triple exponential function. [b] The approximate percent contribution of each lifetime component is in parenthesis. Data was obtained with 375 nm excitation using TCSPC.

Table 2: Fluorescence lifetimes of H6T monomer and THF:water aggregates as a function of emission wavelength.

THF:water	470 nm [a]	490-500 nm	520-530 nm	550 nm	605 nm
	0.27 (80) [b]		0.96 (77.2)	0.96 (85)	1.0 (75)
Monomer	0.92 (18)	-	0.33 (22.6)	0.35 (15)	0.65 (25)
	7.7 (2)		9.7 (0.2)	9.9 (0.1)	10.8 (0.1)
	0.39 (78)	0.42 (59) [d]		1.07 (72)	
1.5:1	1.7 (18)	1.2 (39)	-	0.38 (27)	-
	11.8 (4)	11.7 (2)		11.1 (1)	
	0.36 (79)	0.32 (70) [e]		0.35 (62) [f]	
1:1	1.5 (18)	1.2 (27)	-	1.2 (35)	-
	11.3 (3)	11.0 (3)		11.2 (3)	

[a] All wavelengths are ± 5 nm. [b] The approximate percent contribution of each lifetime component is in parenthesis. [c] Collected at 520 nm. [d] Collected at 500 nm. [e] Collected at 490 nm. [f] Collected at 530 nm. Data was obtained with 375 nm excitation using TCSPC.